

Accelerated Transport through Sliding Dynamics of Rodlike Particles in Macromolecular Networks

Xuanyu Zhang,^{1,2} Xiaobin Dai,^{1,2} Md Ahsan Habib,³ Lijuan Gao,^{1,2} Wenlong Chen,^{1,2} Wenjie Wei,^{1,2} Zhongqiu Tang,³ Xianyu Qi,⁴ Xiangjun Gong,⁴ Lingxiang Jiang,^{3,*} and Li-Tang Yan^{1,2,†}

¹*State Key Laboratory of Chemical Engineering, Department of Chemical Engineering, Tsinghua University, Beijing 100084, China*

²*Key Laboratory of Advanced Materials (MOE), Tsinghua University, Beijing 100084, China*

³*South China Advanced Institute for Soft Matter Science and Technology,*

School of Emergent Soft Matter, South China University of Technology, Guangzhou 510640, China

⁴*Faculty of Materials Science and Engineering, South China University of Technology, Guangzhou 510640, China*

(Dated: April 11, 2023)

Transport of rodlike particles in macromolecular networks is critical for many important biological processes and technological applications. Here, we report that speeding-up dynamics occurs once the rod length L reaches around integral multiple of the network mesh size a_x . Our results clarify that such a fast diffusion of thick rods with commensurate length follows the sliding dynamics and demonstrate it to be anomalous yet Brownian. Moreover, the good agreement between theoretical analysis and simulations corroborates that sliding dynamics is an intermediate regime between hopping and Brownian dynamics, and suggests a mechanistic interpretation based on the rod-length dependent entropic free energy barrier. The findings bring new insight into the physics of the transport dynamics in confined media of networks, and might be of immediate interest to the optimal design of particle transport in diverse networks.

Introduction.—The transport of guest particles in confinement environments of macromolecular networks is important not only as a fundamental problem of soft matter physics, but also as that of materials and biological science: it underlies the behavior of such disparate systems as nanoparticle organization in polymer-network-based nanocomposites [1, 2], selective permeation of bacteria or antibiotics across mucus [3–5], and efficient drug delivery systems targeting tissues covered with extracellular matrix [6–8]. Physically, the dynamics is governed by the corresponding effective free energy landscape contributed by the interaction between particle and networks strands as well as the elastic deformation energy of network strands. For spherical particles, the interplay of these two factors strongly depends on the size ratio between the network mesh and particles, resulting in various diffusion regimes including Brownian, hopping and trapped dynamics [2, 9–13]. However, this simple picture breaks down for rodlike particles because anisotropic shape gives rise to additional competing length scales [14–17]. As various length scales associated with the structure significantly increase the complexity of the dynamics, the fundamental dynamics of such systems is far from established.

In most studies on the transport of rodlike particles in macromolecular networks, rod diameters are much smaller than typical length scales of network meshes [18–22]; the elastic energy due to strand deformation thereby plays a trivial role in the effective free energy landscape. However, the opposite limit, with rod diameter comparable with or even larger than the latter, is ubiquitous. For example, in Fig. S1 we plot the ratio of diameter d to averaged mesh size a_x [illustrated in Fig. 1(a)], d/a_x ,

for a few recent experiments of some typical bacteria in different types of mucus consisting of biomacromolecular networks [23]. The plot clearly demonstrates that d/a_x ranges from about 0.8 to almost 2.0. In this case, the entropic free energy barrier due to the conformational penalty of strands deformed by particles may overwhelm the interactions, leading to new dynamical regimes [24]. Unfortunately, little is known about the physical mechanism regarding the transport of such *thick* rodlike particles in macromolecular networks, leaving an urgent and critical issue to be addressed.

In this Letter, combining simulation, theory and experiment, we study the dynamics of rodlike particles of diameters comparable to mesh size in a cross-linked macromolecular network, in order to unravel the fundamental physics behind the transport in the essential systems. The result has important merits: (1) It reports *speeding-up* longitudinal dynamics occurs once the rod length reaches around integral multiple of the mesh size. (2) It not only reveals that the accelerated transport follows sliding dynamics but also gives the analytical expressions of the time-displacement distribution of sliding dynamics, clarifying its physical relationship with hopping and Brownian dynamics. (3) It allows new principles for the optimal design of particle transport in various networks.

Experiment.—We begin by examining the diffusion behavior of rods with different lengths in the synthetic macromolecular network, where diameters of rods are compared with a_x . The experimental network is polyethylene glycol diacrylate (PEGDA) network, which possesses excellent biocompatibility [25]. PEGDA network is synthesized under ultraviolet (UV) irradiation

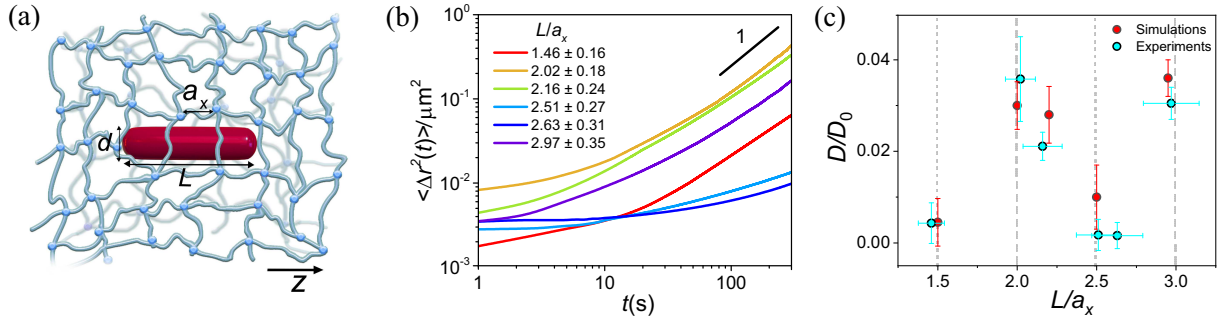


FIG. 1. (a) Schematic of a rodlike particle of diameter d and length L in a macromolecular network with mesh size a_x . (b) $\langle \Delta r^2(t) \rangle$ for different L/a_x in experiments. (c) D/D_0 as a function of L/a_x . The error bars represent the standard deviation.

(see Supplemental Material [23] for more details). a_x of this network is estimated to be $21.0 \pm 1.8 \text{ nm}$ [26, 27]. The experimental rods are PEG-capped Au nanorods (Au-NRs), with lengths ranging from $30.6 \pm 3.4 \text{ nm}$ to $61.4 \pm 7.7 \text{ nm}$ and diameters, including grafted-layer thickness, of around 19.1 nm . To measure the diameter and length of Au-NRs, $2.5 \mu\text{L}$ Au-NR sample is first diluted by dissolving in 0.2 mL ethanol, sonicated for at least 20 min , and then dropped $3\text{-}6 \mu\text{L}$ solution on the transmission electron microscope (TEM) copper grid. After evaporating any solvent on copper grids, we can obtain Au-NR images by TEM with 120 kV acceleration voltage. Rod sizes are measured from the TEM images [Fig. S2], and the averaged values are listed in Table S2.

To determine the trajectories of Au-NRs in the network, the network is filled with $30\mu\text{L}$ Au-NR solution, and is kept for $10\text{-}15 \text{ min}$ on an optical microscope stage at the room temperature. The images of trajectories are taken by using dark field techniques [28]. For rods in water, 400 images are recorded at a frequency of 20 Hz for 20 s . For rods in the network, images are taken at a frequency of 10 Hz [11, 29]. To detect the particles in the image stack, filter-based method is used [30]. Particles trajectories are then obtained by Nearest Neighbor Search tracker, as shown in Fig. S3.

For a quantitative analysis, we first examine the mean square displacement (MSD) $\langle \Delta r^2(t) \rangle = \langle [\vec{r}(t_0 + t) - \vec{r}(t_0)]^2 \rangle$, where \vec{r} is the position vector of the rod at time t . The typical MSDs for a set of L/a_x at $d/a_x = 1.0 \pm 0.1$ are shown in Figs. 1(b) and S4 [31, 32]. Strikingly, the diffusivity of rods significantly depends on the rod length for these thick rods. It can be identified that, when the rod length L reaches around integral multiple of the network mesh size a_x , i.e., $L/a_x = 2.02 \pm 0.18$ and 2.97 ± 0.35 , they exhibit a faster diffusion than the rods with lengths noncommensurate with the mesh size, i.e., $L/a_x = 1.46 \pm 0.16$, 2.51 ± 0.27 and 2.63 ± 0.31 . This indicates that the speeding-up dynamics occurs upon that L reaches around integral multiple of a_x . To further examine this length-dependent speeding-

up behavior, we calculate the D/D_0 , i.e., the ratio between longtime diffusion coefficients in the network and neat solvent [Fig. 1(c)]. Indeed, D/D_0 reaches a maximum for a rod with commensurate length, clarifying this unique dynamical behavior.

The nonmonotonic dependence of the diffusivity on L for thick rods is in sharp contrast to the monotonically decreased diffusivity with the increase of L for thin rods, as reported in both previous works [19] and our simulation results of thin rods [Fig. S5]. Such an exceptional dependence on speeding-up dynamics indicates that the length commensuration is critical for the dynamical behaviors of thick rods, yielding new principles for the optimal design of rodlike particles with highly efficient transport in macromolecular networks. To elucidate the physical origin of the speeding-up dynamics, we turn to the detailed microscopic dynamics of thick rods in macromolecular networks.

Simulation.—Full technical details on the simulation model are described in the Supplemental Material [23] and briefly introduced here. We simulate the transport of a rodlike particle in a cross-linked network using coarse-grained molecular simulations [33]. For all systems, the network mesh size is fixed at $a_x = 3.35r_c$, while various values of d and L are set to consider their roles in the rod dynamics. **r_c is length unit.** Particularly, d is set to be comparable to a_x , ranging from $1.3a_x$ to $1.9a_x$, and L ranges from $1.5a_x$ to $4.4a_x$, with which the off-axis dynamics is negligible [23]. As shown in Fig. 2(a), typical MSDs exhibit the nonmonotonic dependence of the diffusivity on the length commensuration, similar to that in Fig. 1(b). Detailed simulations pertinent to experimental systems also demonstrate this nonmonotonic dependence for D/D_0 , remarkably consistent with experiments [Fig. 1(c)].

To evaluate the generality of such dynamic dependence on the length scales of rod and network, we systematically explore the diffusion behaviors of thick rods as a function of L/a_x and d/a_x , allowing us to construct a diagram of diffusion dynamics in the two-parameter space, as depicted in Fig. 2(b). For each size ratio inter-

val $L/a_x \in [n, n+1]$ with $n = 0, 1, 2, \dots$, the diffusion of rod possesses similar dynamic types. That is, three characteristic regimes can be discriminated as denoted by colored circles in Fig. 2(b): when L is noncommensurate with a_x , the rod diffusion is featured by hopping between neighboring network cells for small d/a_x while it turns to trapped dynamics within a single cell upon about $d/a_x > 1.6$; interestingly, between two neighboring hopping regimes there indeed exists the regime of speeding-up longitudinal dynamics, where L reaches around integral multiple of a_x , corresponding to Fig. 2(a).

In order to provide a detailed insight into the accelerated transport mentioned above, we compare dynamical behaviors in regimes of hopping and speeding-up dynamics through calculating different parameters, i.e., typical trajectories in the direction of \mathbf{z} -axis and the corresponding displacement probability distribution function(DPDF) $G_s(z, t)$ [Fig. 3(a) and (b)]. The trajectory of the rod in the regime of hopping dynamics shows that the rod undergoes constrained motion punctuated by significant large-scale full jumps [Fig. 3(a)]. This can be confirmed from the $G_s(z, t)$ lines where regular peaks emerge and the distance between adjacent peaks is around $1.0a_x$, indicating that the rod jumps from a network cell to its neighboring one. By contrast, in the regime of speeding-up dynamics, the rod that experiences the fast transport dynamics does not exhibit hopping-type events as sharp as those observed for the noncommensurate rod. Instead, only random and local waiting intervals of small scales appear in the trajectory [Fig. 3(b)], resulting in shallow and irregular peaks in lines of $G_s(z, t)$. Clearly, the $G_s(z, t)$ is non-Gaussian, but is different from those of hopping dynamics with regular peaks and Brownian dynamics without any harmonic peak (Fig. S6).

Moreover, the systematic measurement in our ex-

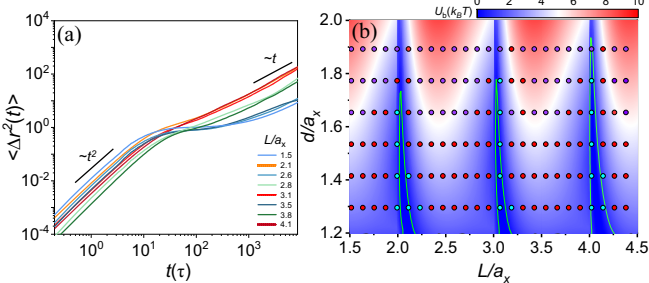


FIG. 2. (a) $\langle \Delta r^2(t) \rangle$ for different L/a_x at $d/a_x = 1.4$. (b) Diagram of rod dynamics interrelating to L/a_x and d/a_x . Circles: simulation results of (red) hopping, (cyan) speeding-up, and (purple) trapped dynamics. The contour map: theoretical results of U_b with various d/a_x and L/a_x . The green lines: boundary (where $U_b = k_B T$) between the speeding-up and hopping regimes, determined by a theoretical model [Eq. (1)]. The color bar at the upper right corner indicates the value of U_b .

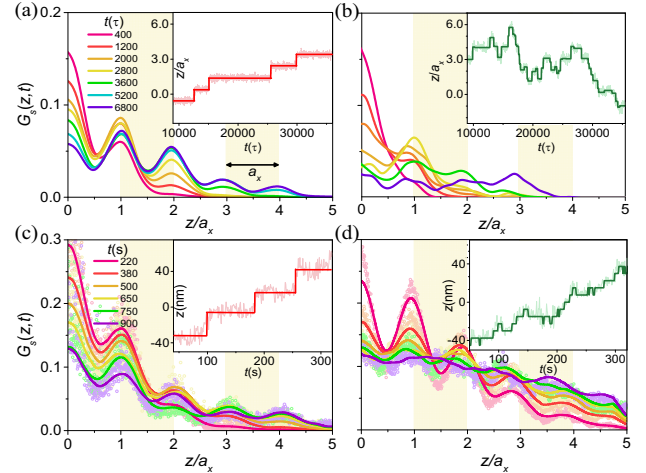


FIG. 3. Simulated $G_s(z, t)$ of rods with (a) $L/a_x = 2.6$ and (b) $L/a_x = 3.1$ at $d/a_x = 1.4$ along \mathbf{z} -axis, showing hopping-type diffusion and speeding-up diffusion respectively. Experimental $G_s(z, t)$ of rods with (c) $L/a_x = 2.51 \pm 0.27$ and (d) $L/a_x = 2.97 \pm 0.35$ corresponding respectively to (a) and (b), where solid lines represent smoothed results of circles. The inset of each panel presents typical trajectory of the center of mass of the corresponding rod, where thin lines represent unsmoothed original displacement while thick lines represent smoothed displacement determined by a wavelet-based method [34].

periments allows us to determine the typical trajectories as well as $G_s(z, t)$ for the commensurate and non-commensurate rods corresponding to those in simulations [Figs. 3(c),(d), S7 and S8]. By comparing Fig. 3(c),(d) to (a),(b) respectively, a good agreement between experimental and simulation results is identified, corroborating the hopping and speeding-up dynamics for the non-commensurate and commensurate rods. The more random fluctuation in the displacement of speeding-up dynamics implies that the rod undergoes a lower free energy barrier, and the thermal noise as well as the strong effect of the local environment may thereby play a nontrivial role.

Theory.—To further pinpoint the physical origin behind the accelerated transport of a rod in a macromolecule network, we develop a theoretical model to analyze the free energy landscape and dynamical regimes depending on the length scales of rod and network. Considering a canonical ensemble of a rod in a macromolecule network, it is specified by (1) the set of cross-links $k = \{\mathbf{r}_i\}_{i=1}^M$, with M cross-links between the efficiently bridged Gaussian chains; (2) the collection of linker connections marked as the tuple (i,j) ; (3) the continue curve path of linked strands $\mathbf{R}_{ij}(s)$ with contour variable $s \in [0, 1]$. For a Gaussian chain of N bonds of Kuhn length b , $a_x = bN^{1/2} = 1$ is the unit length of the system[10]. Through coupling the particle effect into the renowned theory of network elasticity[35, 36], the

partition function of the rod-network system takes the form[23]:

$$Z(\mathbf{r}_{rod}, \mathbf{l}_{rod}) = \prod_k \int d\mathbf{r}_k \prod_{(i,j)} \int \mathcal{D}\mathbf{R}_{ij} \delta(\mathbf{r}_i - \mathbf{R}_{ij}(0)) \quad (1)$$

$$\times \delta(\mathbf{r}_j - \mathbf{R}_{ij}(1)) e^{-\sum_{i,j} \left[\int_0^1 ds \frac{3}{2N b^2} \|\mathbf{u}_{ij}\|^2 + U_{mr}(\mathbf{R}_{ij}, \mathbf{r}_{rod}, \mathbf{l}_{rod}) \right]}$$

where $\mathbf{u}_{ij} = d\mathbf{R}_{ij}/ds$ is the tangent direction of a network strand, \mathbf{r}_{rod} and \mathbf{l}_{rod} give the position and direction of the rod, δ is the delta function, $\beta = 1/k_B T$, k_B is the Boltzmann constant, and T is temperature. U_{mr} represents the hard-core monomer-rod interaction [23]. The free energy of the rod-network system has the form $F(\mathbf{r}_{rod}, \mathbf{l}_{rod}) = -k_B T \ln Z(\mathbf{r}_{rod}, \mathbf{l}_{rod})$. To quantitatively examine the free energy experienced by the rod, the free energy change is defined as $\Delta F(\tilde{z}) = F(\tilde{z}) - F^{min}(\tilde{z})$, where \tilde{z} is the position of rod center as denoted by the coordinate in Fig. 4(c), and $F^{min}(\tilde{z})$ represents the minimum free energy along \mathbf{z} -axis.

We calculate some typical profiles of ΔF as a function of \tilde{z}/a_x for various d/a_x at $L/a_x = 1.5$ and 2.0, corresponding respectively to the noncommensurate and commensurate rods [Figs. 4(a) and (b)]. Intuitively, ΔF depends on the number and deformation degree of loops around a rod. As illustrated by the schematic in Fig. 4(c), ΔF reaches the maximum at the network cell center with $\tilde{z} = 0$, and the minimum at the network cell edge with $\tilde{z} = 0.5a_x$. Then, the height of the free energy barrier for the transition of the rod is $U_b = \Delta F^{max}(\tilde{z}) - \Delta F^{min}(\tilde{z})$, where $\Delta F^{max}(\tilde{z})$ is the maximum of $\Delta F(\tilde{z})$. In view of the Kramers' escape theory[37], the noncommensurate rod facing a barrier of $U_b > k_B T$ [Fig. 4(a)] should possess hopping dynamics, consistent with simulation results in Fig. 3(a). However, it is emphasized that the commensurate rod cannot give rise to hopping dynamics but a speeding-up dynamics with fast diffusion due to much

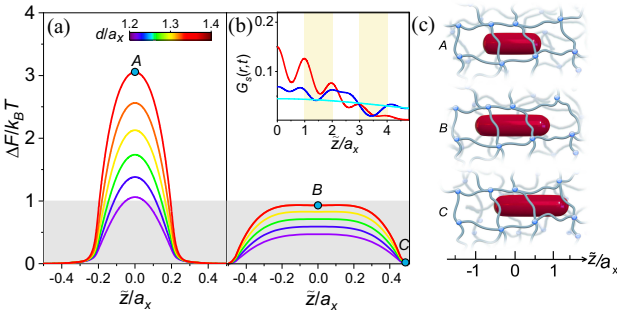


FIG. 4. ΔF as a function of \tilde{z} for various d/a_x , where $L/a_x = 1.5$ (a) and 2.0 (b). The color bar indicates the value of d/a_x . Typical positions of rod center for various L/a_x are schematically illustrated in (c): A. $\tilde{z}/a_x = 0$, $L/a_x = 1.5$; B. $\tilde{z}/a_x = 0$, $L/a_x = 2.0$; C. $\tilde{z}/a_x = 0.5$, $L/a_x = 2.0$. The inset in (b): theoretical results of $G_s(\tilde{z}, t)$ for (red) hopping, (blue) sliding and (cyan) Brownian dynamics.

lower barrier of $0 < U_b < k_B T$, as marked by the shaded region in Fig. 4(b). To further assess how the free energy barrier U_b relates to the dynamical regimes of hopping and speeding-up dynamics, we systematically calculate U_b for the same ranges of d/a_x and L/a_x with those in Fig. 2(b), allowing us to construct U_b landscape plotted by the colored contour map in the d/a_x - L/a_x plane. As indicated by the color map in Fig. 2(b), the landscape clarifies a strong dependence of dynamical regimes on U_b : hopping and trapped regimes take place within the range of $U_b > k_B T$ for noncommensurate rods; between two neighboring hopping regimes, there is a valley of $0 < U_b < k_B T$ for commensurate rods, corresponding to the speeding-up dynamics. Moreover, the definite boundary of $U_b = k_B T$ is plotted, distinguishing the detailed ranges of speeding-up dynamics around integral multiple of L/a_x .

The fairly smooth landscape reveals that the speeding-up dynamics really follows the sliding dynamics characterized by the energy barrier of order of $k_B T$ and emerging predominantly in the diffusion of proteins along DNA [38–40]. Our simulations demonstrate that in such unique dynamics, MSD is simply proportional to time (Fickian), yet the DPDF is not Gaussian as should be expected of a classical random walk, bearing great resemblance to the “anomalous yet Brownian” diffusion as found in some crowded fluids [41, 42].

Based on the calculations of the free energy landscape, we extend the theoretical analysis to microscopic dynamics to provide a refined picture of these dynamical regimes [23]. Fundamentally, the distribution of the total number of network cells traversed can be obtained in Fourier-Laplace space from the Montroll-Weiss equation [43],

$$S(k, s) = \frac{1 - \tilde{\psi}(s)}{s \left[1 - \hat{\phi}(k) \tilde{\psi}(s) \right]} \quad (2)$$

where $S(k, s)$ is the Fourier-Laplace transform of $G_s(\tilde{z}, t)$, $\hat{\phi}(k)$ and $\tilde{\psi}(s)$ are the respective Fourier and Laplace transforms of $\phi(\tilde{z})$, $\psi(t)$, denoting the waiting time and jump length distribution, respectively. The detailed forms of $G_s(\tilde{z}, t)$ in the dynamical regimes are different, depending on U_b . Our following discussions are thereby based on the aforementioned regimes of U_b .

For high barriers of $U_b > k_B T$, we choose $\psi(t) = (1/\tau_{hop}) \exp(-t/\tau_{hop})$, and $\phi(\tilde{z}) = NP(n)\delta(|\tilde{z}| - na_x)$ derived by Mel'nikov[44], where τ_{hop} is the characteristic hopping time[23], $P(y) = \exp(-4\beta U_0 y^2/a_x^2)$ gives the Boltzmann distribution, n is an integral number, and N is the normalization constant such that $\sum_{n=0}^{\infty} NP(n) = 1$. Thus, one can deduce that for large time scales, it takes the form,

$$G_s(\tilde{z}, t) = (\tau_{hop}/4\pi a_x^2 t)^{1/2} \exp(-\tau_{hop}\tilde{z}^2/4ta_x^2) \phi(\tilde{z}) \quad (3)$$

where the exponential tails prevail. As the red curve in the inset of Fig. 4(b), the plot of G_s exhibits an identical

shape as expected to the hopping dynamics shown in Fig. 3(c).

For low barriers of $0 < U_b < k_B T$, a master equation is applied to respect the nonlocal nature of irregular peaks in $G_s(\tilde{z}, t)$, which takes the form[23], $G_s(\tilde{z}, t) = G_s(\tilde{z}, 0) + \int_0^t \sum_{\tilde{z}'} \omega(\tilde{z} - \tilde{z}') G_s(\tilde{z}', t') dt$, where the kernel $\omega(\tilde{z})$ has the standard Poisson random measure[41, 45]. Then, the DPDF gives,

$$G_s(\tilde{z}, t) = 4 \exp(-2|\tilde{z}|/a_x) \exp(-2t/\tau_{hop}) \quad (4)$$

$$\times \int_0^\infty dx \exp(-4x/a_x) I_0\left(\sqrt{\frac{8t(|\tilde{z}|+x)}{a_x\tau_{hop}}}\right) I_0\left(\sqrt{\frac{8tx}{a_x\tau_{hop}}}\right)$$

where I_0 is the modified Bessel function of the first kind. Here we plot the blue curve of $G_s(\tilde{z}, t)$ in the inset of Fig. 4(b), demonstrating the random distribution of peaks resembling the sliding dynamics shown in Fig. 3(d).

For no barrier of $U_b = 0$, the solution of Eq. (2) is $G_s(\tilde{z}, t) = (\tau_0/4\pi a_x^2 t)^{1/2} \exp(-\tau_0 \tilde{z}^2/4ta_x^2)$. As shown by the cyan curve in the inset of Fig. 4(b) the theoretical result is consistent with the simulated curve at the late stage (Fig. S5) [23], reflecting the Gaussian distribution of Brownian dynamics.

Conclusion.—We found that by tuning the rod length with respect to the averaged mesh size speeding-up longitudinal dynamics occurs once the rod length reaches around integral multiple of the mesh size. We identified that the accelerated transport follows sliding dynamics which is demonstrated to be anomalous yet Brownian. We further gave the analytical expression of time-displacement distribution of sliding dynamics and clarified its physical relationship with hopping and Brownian dynamics. Our results revealed that the transition of these dynamical regimes is fundamentally attributed to the rod-length dependent free energy barrier originated predominantly from the entropic contribution due to the conformational penalty of strands deformed by thick rods, in contrast to the rigorous periodic potential [14, 17]. The findings are of immediate interest to the optimal design of particle transport in various networks, biological or synthetic. As similar landscape of free energy is experienced by both passive and active rods in the confined environment of macromolecular networks, we speculate that the dependence of transport dynamics on size commensuration can be extended to the active case, providing the fundamental cornerstone for the further understanding of these nonequilibrium phenomena.

We thank Pengyu Chen for stimulating discussion. We acknowledge support from National Natural Science Foundation of China (Grant Nos. 22025302, 21873053 and 22122201). L.-T. Y. acknowledges financial support from Ministry of Science and Technology of China (Grant No. 2022YFA1200061).

X. Z., X. D., and M. A. H. contributed equally.

* jianglx@scut.edu.cn

† ltyan@mail.tsinghua.edu.cn

-
- [1] M. L. Gardel, J. H. Shin, F. MacKintosh, and C. Ma-hadevan, *Science* **304**, 1301 (2004).
 - [2] E. J. Bailey and K. I. Winey, *Prog. Polym. Sci.* **105**, 101242 (2020).
 - [3] O. Lieleg and K. Ribbeck, *Trends Cell Biol.* **21**, 543 (2011).
 - [4] O. Alvaro, F. Sabrina, and A. Sonja-Verena, *Annu. Rev. Microbiol.* **67**, 337 (2013).
 - [5] B. Button, L. H. Cai, C. Ehre, M. Kesimer, D. B. Hill, J. K. Sheehan, R. C. Boucher, and M. Rubinstein, *Science* **337**, 937 (2012).
 - [6] A. D. Theocaris, S. S. Skandalis, C. Gialeli, and N. K. Karamanos, *Adv. Drug Delivery Rev.* **97**, 4 (2016).
 - [7] R. G. Thorne, A. Lakkaraju, E. Rodriguez-Boulan, and C. Nicholson, *Proc. Natl. Acad. Sci. U.S.A.* **105**, 8416 (2008).
 - [8] E. Fröhlich and E. Roblegg, *Adv. Drug Delivery Rev.* **61**, 158 (2009).
 - [9] L. H. Cai, S. Panyukov, and M. Rubinstein, *Macromolecules* **48**, 847 (2015).
 - [10] Z. Xu, X. Dai, X. Bu, Y. Yang, X. Zhang, X. Man, X. Zhang, M. Doi, and L.-T. Yan, *ACS Nano* **15**, 4608 (2021).
 - [11] I. Y. Wong, M. L. Gardel, D. R. Reichman, E. R. Weeks, M. T. Valentine, A. R. Bausch, and D. A. Weitz, *Phys. Rev. Lett.* **92**, 178101 (2004).
 - [12] Z. E. Dell and K. S. Schweizer, *Macromolecules* **47**, 405 (2014).
 - [13] X. Dai, X. Zhang, L. Gao, Z. Xu, and L.-T. Yan, *Nat. Commun.* **13**, 4094 (2022).
 - [14] M. Chiappini, E. Grelet, and M. Dijkstra, *Phys. Rev. Lett.* **124**, 087801 (2020).
 - [15] Y. Han, A. M. Alsayed, M. Nobili, J. Zhang, T. C. Lubensky, and A. G. Yodh, *Science* **314**, 626 (2006).
 - [16] T. Bhattacharjee and S. S. Datta, *Nat. Commun.* **10**, 2075 (2019).
 - [17] L. Alvarez, M. P. Lettinga, and E. Grelet, *Phys. Rev. Lett.* **118**, 178002 (2017).
 - [18] J. Choi, M. Cargnello, C. B. Murray, N. Clarke, K. I. Winey, and R. J. Composto, *ACS. Macro. Lett.* **4**, 952 (2015).
 - [19] J. Wang, T. C. O'Connor, G. S. Grest, Y. Zheng, M. Rubinstein, and T. Ge, *Macromolecules* **54**, 7051 (2021).
 - [20] N. Fakhri, F. C. MacKintosh, B. Lounis, L. Cognet, and M. Pasquali, *Science* **330**, 1804 (2010).
 - [21] A. Karatrantos, R. J. Composto, K. I. Winey, and N. Clarke, *Macromolecules* **52**, 2513 (2019).
 - [22] M. Yu, J. Wang, Y. Yang, C. Zhu, Q. Su, S. Guo, J. Sun, Y. Gan, X. Shi, and H. Gao, *Nano Lett.* **16**, 7176 (2016).
 - [23] See Supplemental Material for additional methods, analysis, and figures.
 - [24] E. Yamamoto, T. Akimoto, A. Mitsutake, and R. Metzler, *Phys. Rev. Lett.* **126**, 128101 (2021).
 - [25] V. Hagel, T. Haraszti, and H. Boehm, *Biointerphases* **8**, 36 (2013).
 - [26] M. Molaei, E. Atefi, and J. C. Crocker, *Phys. Rev. Lett.* **120**, 118002 (2018).
 - [27] T. Canal and N. A. Peppas, *J. Biomed. Mater. Res.* **23**, 1183 (1989).

- [28] J. Schindelin, I. Arganda-Carreras, E. Frise, V. Kaynig, M. Longair, T. Pietzsch, S. Preibisch, C. Rueden, S. Saalfeld, B. Schmid, *et al.*, Nat. Methods **9**, 676 (2012).
- [29] M. T. Valentine, P. D. Kaplan, D. Thota, J. C. Crocker, T. Gisler, R. K. Prud'homme, M. Beck, and D. A. Weitz, Phys. Rev. E **64**, 061506 (2001).
- [30] J. C. Crocker and D. G. Grier, J. Colloid Interface Sci. **179**, 298 (1996).
- [31] K. A. Rose, M. Molaei, M. J. Boyle, D. Lee, J. C. Crocker, and R. J. Composto, J. Appl. Phys. **127**, 191101 (2020).
- [32] M. Gardel, M. Valentine, and D. Weitz, Microrheology, in *Microscale Diagnostic Techniques*, edited by K. S. Breuer (Springer Berlin Heidelberg, Berlin, Heidelberg, 2005) pp. 1–49.
- [33] R. D. Groot and P. B. Warren, J. Chem. Phys. **107**, 4423 (1997).
- [34] K. Chen, B. Wang, J. Guan, and S. Granick, ACS Nano **7**, 8634 (2013).
- [35] R. Deam and S. F. Edwards, Phys. Trans. R. Soc. **280**, 317 (1976).
- [36] F. Schmid, Phys. Rev. Lett. **111**, 028303 (2013).
- [37] P. Hänggi, P. Talkner, and M. Borkovec, Rev. Mod. Phys. **62**, 251 (1990).
- [38] C. Loverdo, O. Benichou, R. Voituriez, A. Biebricher, I. Bonnet, and P. Desbiolles, Phys. Rev. Lett. **102**, 188101 (2009).
- [39] J. Gorman and E. C. Greene, Nat. Struct. Mol. Biol. **15**, 768 (2008).
- [40] M. Slutsky and L. A. Mirny, Biophys. J. **87**, 4021 (2004).
- [41] B. Wang, J. Kuo, S. C. Bae, and S. Granick, Nat. Mater. **11**, 481 (2012).
- [42] B. Wang, S. M. Anthony, S. C. Bae, and S. Granick, Proc. Natl. Acad. Sci. U.S.A. **106**, 15160 (2009).
- [43] E. W. Montroll and G. H. Weiss, J. Math. Phys. **6**, 167 (1965).
- [44] V. Mel'nikov, Phys. Rep. **209**, 1 (1991).
- [45] J. Bisquert, Phys. Rev. Lett. **91**, 010602 (2003).